Atmospheric Environment 206 (2019) 60–71

Contents lists available at ScienceDirect

Atmospheric Environment

journal homepage: www.elsevier.com/locate/atmosenv

Effect of aqueous-phase processing on the formation and evolution of organic aerosol (OA) under different stages of fog life cycles

Anil Kumar Mandariya[a], Tarun Gupta[a,b,*], S.N. Tripathi[a,b,**]

[a] Department of Civil Engineering, Indian Institute of Technology, Kanpur, India
[b] Centre for Environmental Science and Engineering, IIT, Kanpur, India

GRAPHICAL ABSTRACT

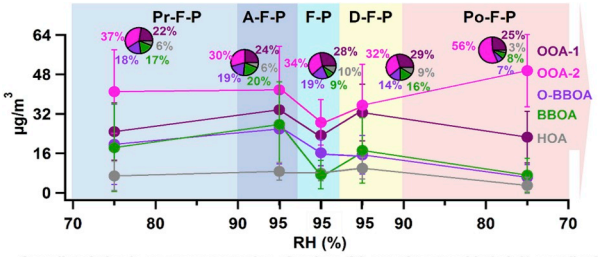

Overall variation in mass concentration of various OA constituents with their % contribution into OA during various fog processing periods in Kanpur at the central Indo-Gangetic Plain

ARTICLE INFO

Keywords:
Fog
SOA
Fog processing periods
Fragmentation
Oligomerization
Functionalization
O/C ratio

ABSTRACT

Secondary organic aerosol (SOA) is a significant component of organic aerosol (OA), formed majorly via aqueous-phase processing (aqSOA) during winter fog period yet it persist as a significant source of uncertainties within climate models due to lack of sufficient knowledge about its ambient formation and evolution processes. Kanpur is situated at the center of Indo-Gangetic Plain which witnesses several fog episodes every year during winter time. In this study, we have evaluated the effect of aqueous-phase processing on the formation pathway of OA, its composition and oxidative properties during five fog processing periods, i.e., Pre-Fog-Period (Pr-F-P), Activating-Fog-Period (A-F-P), Fog-Period (F-P), Dissipating-Fog-Period (D-F-P), and Post-Fog-Period (Po-F-P). A-F-P was observed as heavily polluted period (249.8 ± 47.8 μg/m^3) while F-P period was least polluted (153.1 ± 37.8 μg/m^3) indicating the wet removal through grown fog droplets. Oxygenated organic aerosol (OOA-1) processed mainly through biomass burning (BB) emission suggesting is a good surrogate of aqueous SOA, and it gets enhanced significantly during high biomass-burning emissions during A-F-P and D-F-P under acidic aerosol conditions. Also, in contrast to formation mechanism, our results proposing specific formation process (fragmentation, functionalization, or oligomerization) for different fog processing periods. A-F-P and D-F-P periods are crucial possibly for the formation of OA dominant through oligomerization mechanism in which functionalization of −OH moieties occurs in A-F-P periods, whereas oligomerization mechanism with the addition of carbonyl (aldehyde/ketone) moieties could occur in D-F-P periods, accompanied by acidic aerosol as well as high aerosol liquid water content (ALWC). In contrast, during OA evolution process, Van Krevelen (VK) slope, O/C ratio, SOA O/C ratio (O/C_{OOA}), average oxidation state of carbon for bulk-aerosol (OS_C) and SOA $(OS_C)_{OOA}$, substantially varies throughout all the fog processing periods.

* Corresponding author. Department of Civil Engineering, Indian Institute of Technology, Kanpur, India.
** Corresponding author. Centre for Environmental Science and Engineering, IIT, Kanpur, India.
E-mail addresses: tarun@iitk.ac.in (T. Gupta), snt@iitk.ac.in (S.N. Tripathi).

https://doi.org/10.1016/j.atmosenv.2019.02.047
Received 15 November 2018; Received in revised form 14 February 2019; Accepted 24 February 2019
Available online 08 March 2019

1. Introduction

Understanding the interactions of sub-micron ambient aerosol particles (PM_1, aerodynamic diameter ≤ 1 μm) with atmospheric water is important as it affects the human health (Haddrell et al., 2015), climate through aqueous oxidation and wet removal of atmospheric aerosol (Gilardoni et al., 2014), direct and indirect radiative forcing (France et al., 2013), and visibility (Deng et al., 2016; Shen et al., 2015). Majority of organic aerosol (OA) is confined in the sub-micron size aerosols. OA is made up of plenty of compounds with enormously different properties such as hygroscopicity, volatilities, and degree of oxidation, and it accounts for a significant mass fraction of submicron aerosols (20–80%) (Ervens et al., 2011; Hallquist et al., 2009; Jimenez et al., 2009a,b). OA can be either primary (from direct emission) or secondary origin (formed as a result of atmospheric chemical reactions of their precursor volatile organic compounds (VOCs)). Ambient observations specify that processed, secondary OA (SOA), dominates over primary OA worldwide (Chakraborty et al., 2015; Hallquist et al., 2009; Xu et al., 2016; Zhang et al., 2007). Worldwide estimates indicate that SOA contributes up to 76% in OA (Hallquist et al., 2009).

Estimates of global SOA budget are still largely uncertain due to poor understanding of SOA formation and its evolution pathways, especially in the heavily polluted region in which biomass burning (BB) sources dominate under high relative humidity (RH) and lower temperature (T) conditions. However, OA exhibit various phases (liquid, semisolid, or amorphous solid) depending upon prevailing ambient temperature and RH (Koop et al., 2011). Under high RH conditions, BBOA undergoes a moisture-induced phase transition transforming it from an amorphous semisolid to a liquid phase. Moreover, in fog processing scenario, bulk diffusion coefficients of OH and levoglucosan (a marker of BBOA) enhance as compared to dry atmospheric conditions (Arangio et al., 2015). These have subsequent effects on the SOA production due to changes in the diffusivity of oxidant and organics. In addition, recent studies in winter time at the similar sampling location have found BB to be a dominant player in the SOA formation during fog processing (Chakraborty et al., 2016c, 2015; Choudhary et al., 2018; Kaul et al., 2012, 2011; Satish et al., 2017; Shamjad et al., 2016) and found that SOA formation is affected by various factors like T, RH (Donahue et al., 2006; Xu et al., 2016), fog (Frank et al., 1998) and OA loading (Chakraborty et al., 2016c).

However, the direct quantification of SOA in ambient environments is challenging, but recent studies based on aerodyne aerosol mass spectrometer (Canagaratna et al., 2007; DeCarlo et al., 2006) and oxygenated OA (OOA) quantified with PMF (positive matrix factorization) (surrogate of SOA) (Wu et al., 2018; Zhang et al., 2007) have shown a better approach for evolution of OA in real time (Chakraborty et al., 2015; Hallquist et al., 2009). Therefore, worldwide OOA is used to study the evolution and formation pathway of SOA (Chakraborty et al., 2015; Chen et al., 2011; Gelencsér et al., 2007; Gilardoni et al., 2014, 2016; Jimenez et al., 2009a,b; Li et al., 2013; Lim et al., 2010; McNeill, 2015; Sun et al., 2013). The SOA could form through gas-phase photochemical oxidation (Herndon et al., 2008; Robinson et al., 2007, 2006), heterogeneous reactions (McNeill, 2015; Rajput et al., 2016a) or aqueous phase oxidation in wet aerosols, clouds, and fogs (Chakraborty et al., 2016a, 2015; Ervens et al., 2011; Ge et al., 2012; Kaul et al., 2011; Singh and Gupta, 2016; Wu et al., 2018; Xu et al., 2017). Many field studies have been conducted during winter time in the past to evaluate the OA as well as SOA during haze and fog. For example, Gilardoni et al. (2016) have shown evidence of aqueous processing of primary BBOA, and observed aqueous SOA (aqSOA) from BBOA, mainly through its strong correlation with ALWC, and presence of guaiacol dimer signature in its mass spectra (Gilardoni et al., 2016). Although Sun et al., 2016 (Sun et al., 2016), signifies the impact of aqueous-phase processing on the highly oxidized OA and freshly oxidized OA during winter in Beijing. However, these studies did not specify the effects of aqueous-phase processing on biomass burning aerosol and OA composition during different fog processing periods. Kaul et al. (2011) (Kaul et al., 2011) linked fog episodes as a marker of aqueous-phase processing at this location and found enhancement of SOA during this periods. Gupta and Mandariya (2013) (Gupta and Mandariya, 2013) also found enhancement of PM_1 mass loading during foggy days as compared to non-foggy days in Kanpur. Further, Chakraborty et al. (2015) (Chakraborty et al., 2015) points out the relative importance and contribution of fresh biomass burning organic aerosol (BBOA) and aged BBOA in OA during foggy and non-foggy periods with pre-fog, fog, and post-fog in winter at the current study site. They also suggest the different aging mechanism in these periods by observing different Van Krevelen slopes. Also, Chakraborty et al., (2016c) (Chakraborty et al., 2016c) observed that fog reduced the negative impact of loading on oxidation of OA at the same location in the winter time. However, they limited their study to pre-fog, fog, and post-fog periods and comparisons were made with same time duration of non-foggy days, these periods were classified based on common observation of all fog episode's start and end local time. Rajput et al. (2018) (Rajput et al., 2018) further found enhancement in organic carbon to elemental carbon (OC/EC) ratio, water-soluble organic carbon to organic carbon (WSOC/OC) ratio and organic matter (OM) from non-foggy to foggy periods and indicated the importance of fog processing during winter at the current location.

Although these studies provide the critical insights into the fog and aqueous-phase processing on OA properties and its PMF factors, significant uncertainties of the relative importance of RH and different fog processing periods on the OA formation, its oxidative properties, and transformation still exist. Fog duration varies from minutes to several hours, highly depending on local metrological parameters like RH, temperature and wind speed. Also, these parameters change with time of the day. Therefore, to completely understand the fog processing phenomena as well as its effect on the OA formation pathway and oxidative properties, relatively more number of stages during the fog-cycle are required. Moreover, none of these studies have been carried out to evaluate the combined effect of RH and aqueous-phase processing on OA and SOA. Also, its evolution process during different fog processing periods including activating-fog-period (Pre fog formation period) and dissipating-fog-period (fog dissipation period) have not been studied when BB is dominant. Also, activation fog period and dissipating fog periods represent the period just before (fog formation) and after (evaporation of fog droplets) the fog period, where number concentration of fine droplets, as well as ALWC are higher. These fine droplets and high ALWC provide relatively larger surface area to the incoming BB aerosols as well as soluble VOCs. Activation-fog-period and dissipating-fog-period are crucial for this study in order to separate the combined effect of high ALWC and LWC during pre-fog-period and contrast it with post-fog-period having low ALWC and zero LWC.

2. Material and methods

2.1. Measurement site, study period and instruments

Ambient measurements were carried out in the city of Kanpur (26.5°N, 80.3°E, and 142 m above mean sea level), located in the center of Indo-Gangetic Plain (IGP), from 30th December 2015 to 23rd January 2016. The main PM_1 sources in this region during wintertime include mostly biomass burning, industrial emission, crustal dust, coal combustion, secondary aerosol, vehicular emission, leather tanning industries, domestic fuel combustion and brick kilns (Chakraborty and Gupta, 2010; Gupta and Mandariya, 2013; Rai et al., 2016; Rajput et al., 2018, 2016b). We observed four fog episodes throughout the entire study period while most days were having high relative humidity. Entire fog life cycles observed during the study duration were partitioned into five fog processing periods namely Pre-Fog-Period (Pr-F-P), Activating-Fog-Period (A-F-P), Fog-Period (F-P), Dissipating-Fog-Period (D-F-P), and Post-Fog-Period (Po-F-P). The beginning and end of F-P was

characterized by having a liquid water content (LWC) $\geq 80\ mg/m^3$ and $< 80\ mg/m^3$, respectively for ≥ 5 min (Chakraborty et al., 2015; Gilardoni et al., 2014). The Pr-F-P and Po-F-P were characterized by the before and after F-P period with 60% ≤ RH < 90%, respectively, whereas A-F-P, and D-F-P by before and after F-P period with RH ≥ 90% and LWC $< 80\ mg/m^3$ (for > 5 min), respectively. Pr-F-P included mostly from evening 17:15 h to midnight whereas Po-F-P included mostly afternoon time 11:00 h to 15:00 h. A-F-P period generally included late night time whereas D-F-P period included the morning time 08:30 h to 11:00 h. The F-P period was occurring mostly in the early morning time.

An HR-ToF-AMS (AMS) (Canagaratna et al., 2007; DeCarlo et al., 2006) was deployed to measure the chemical composition of non-refractory particles of vacuum aerodynamic diameter less than 1 μm (NR-PM_1) at 2 min resolution using high-sensitivity V-mode. The ambient aerosol were dried (RH < 15%) by a diffusion silica-gel dryer before entering into the AMS. AMS measurement represents the interstitial aerosols, unactivated droplets and residual aerosols left behind after fog evaporates in polluted fog (Frank et al., 1998). The AMS was calibrated for ionization efficiency (IE), and particle sizing following standard procedure (Drewnick et al., 2005; Jayne et al., 2000; Jimenez et al., 2003). Periodically IE calibrations were performed before, during, and after the experiment using NH_4NO_3 aerosol. Furthermore, High-efficiency particle arrestance/zero particle filter measurements were made at intervals of 2–3 days and during IE calibrations to assess the presence of gaseous interference in the mass spectra. The liquid water content of fog droplets was measured with a cloud combination probe (CCP, Droplet Measurement Technologies) at the rooftop of the laboratory building (at the height of 10 m above ground level). The details of CCP deployment can be found elswhere (Chakraborty et al., 2016b). The meteorological conditions during complete study period like ambient relative humidity (RH) and temperature were observed by using a collocated temperature and RH sensor (Vaisala, Inc. Humicap, the HMT337 accuracy of ± 1% for RH < 90%) whereas wind speed and direction, boundary layer height, pasquill stability class, horizontal and vertical mixing coefficient data were obtained from NOAA ARL dataset.

The detailed data analysis has been described in supplementary information.

3. Result and discussion

3.1. Average meteorological parameters for fog processing periods

As illustrated in Fig. S7, current study site gets mainly influenced by surface emission sources. Four fog life cycles were observed during the entire study period. 1st, 2nd, 3rd, and 4th fog life cycles were observed at 1st, 15th, 22nd, and 23rd January, respectively. During different fog periods, atmosphere varied from neutral to extremely stable conditions as illustrated in Table 1. The wind rose plot (Fig. S10(a)) shows the wind speeds and directions during fog life cycles. Overall, the prevailing surface wind directions were north-north westerly and north-north easterly, and these sectors accounted for ~65% and ~35% respectively of the total wind frequencies. Wind speeds were found to be ranging from 0.5 to 3.1 m/s (1.9 ± 0.7 m/s), which results in a stable atmospheric condition. Further to investigate the potential for the horizontal advection of OA factors, we also examined the relationships between loading of various OA factors, ventilation coefficient (VC), and wind speed and wind direction using the bivariate polar plot. VC can be considered as an essential parameter over a region of interest as it played a crucial role in describing the dilution and dispersion of the aerosol (Rai et al., 2016). The average value of VC ($585.2\ m^2/s$) observed, was lower than of 3 winter season (2008–09 to 2011–12) reported for the same site (Rai et al., 2016). Also, observed value is less than of $2000\ m^2/s$ for this study area (Fig. S10(b)) which indicates the "bad" category (Eagleman, 1996) from pollution dispersion point of view during various fog life cycles. Thus, comparatively dominant air masses along with higher wind speed and VC from the west-northwest sector significantly contribute in accumulating the OA toward relatively lower VC and wind speed. The higher concentrations of OOA-1 are associated with low wind speeds (Fig. S10(c)), and low VC values suggest that OOA-1 formation is most likely of local origin. The overall averaged RH (%), T (°C), WS (wind speed), WD (wind direction), and LWC (shown for only Pr-F-H, F, and Po-F-H) for all fog processing periods of fog life cycles are reported in Table 2. Generally, fog formation starts under the saturated ambient air condition (RH ~ 100%) and persists for a long time under relatively stable atmosphere. However, some recent investigations (Chakraborty et al., 2015; Gupta and Mandariya, 2013; Kaul et al., 2011; Li et al., 2013; Meng et al., 2014; Singh and Gupta, 2016) have observed it even at a relatively lower RH values, and also Deng et al. (2008) found that it can explained by at least 5% of negative bias of measurement instrument working under extremely high RH.

3.2. Effect of aqueous-phase processing on NR-PM_1, its species and OA during the various fog-processing periods

The campaign overview is carefully described in supplementary (figure S2 (a, b, c, d, e, and f) and related text).

Fig. 1(a and b, and c) shows dynamic variation of overall mass concentration and fraction mass of NR-PM_1 species and organic aerosol (OA) components for different fog processing periods of fog life cycles. The NR-PM_1 showed a very significant ($p < 0.05$) variation thought all periods including highest during A-F-P period (249.8 ± 47.8 $\mu g/m^3$) while lowest during F-P period (153.1 ± 37.8 $\mu g/m^3$), this variation can be attributed to the variation of various species as shown in Fig. 1 (a). Among all NR-PM_1 species, OA increases significantly ($p < 0.05$) with higher rate (27.8%) followed by Cl^- (25.5%), NO_3 (20.4%), and NH_4 (9.8%) except SO_4 which slightly decreases (0.03%) insignificantly ($p > 0.05$) initially from Pr-F-P to A-F-P period. However, during transition from A-F-P to F-P period, all species loading decreases significantly ($p < 0.05$). Further, high RH and lower T during A-F-P enhances the condensation process and provides a greater driving force to grow the accumulation mode particles via condensation (Seinfeld and Pandis, 2006). ALWC is a ubiquitous aerosol constituent in the atmosphere that is present in the condensed phase as a function of relative humidity (RH), temperature, aerosol concentration and chemical composition (Zhou et al., 2011). Field investigations confirm the ubiquity of the metastable state of ambient aerosol (Nguyen et al., 2015), in which water is always present. In humid locations, ALWC is an abundant medium available to partition polar, water-soluble gas phase organic gases to the condensed phase (Parikh et al., 2011) to facilitate SOA formation and contribute to the atmospheric PM load (Carlton and Turpin, 2013; Hodas et al., 2015). Also, ALWC increases (Table 2) exponentially with RH (Xu et al., 2017) as it play a key role in condensation process and aqueous-phase reactions. Aerosol provides sufficient surface area for condensation of atmospheric water vapor to form droplets and these droplets eventually grow slowly such that A-F-P becomes persistent (Singh et al., 2011). However, in the current study 83.2% grown droplets were from fine droplet mode (Table 2), and thus the possibility of wet scavenging of interstitial aerosols by these tiny droplets is quite less. Whereas, the aqueous-phase oxidation reactions simultaneously enhance both organic and inorganic species mass within interstitial aerosols (Kaul et al., 2011) as well as within the droplets (Ervens et al., 2011). A good correlation ($R^2 = 0.71$, $p < 0.01$, RH ≤ 93%) of NR-PM_1 with ALWC as shown in Fig. S8, indicate the enhancement in the aerosol mass possibly due to aqueous-phase processing (Xu et al., 2016). Non-significant ($p > 0.05$) change in SO_4 mass concentration suggested presence and dominance of its constant source. Also, other inorganic species (NO_3, NH_4, and Cl) followed a similar trend as OA (Fig. 1(a)) during Pr-F-P to A-F-P period. The lower temperature, higher RH, and high ALWC during A-F-P period, further suggest the enhancement in thermodynamically driven gas/particle partitioning of nitrate (Seinfeld and Pandis, 2006),

Table 1
Averaged (± standard deviation) meteorological parameters (wind speed (WS), wind direction (WD), solar radiation (SR), planetary boundary layer (PBL), pasquill stability class (PSQ, C: slightly unstable, D: neutral, E: slightly stable, F: moderately stable, G: extremely stable), vertical mixing coefficient (K_z), horizontal mixing coefficient (K_h), relative humidity (RH), temperature (T)) in different stages of all fog life cycles.

FOG LIFE CYCLE	FOG PROCESSING STAGE	WS (M/S)	WD (° FROM N)	SR (W/M^2)	PBL (M)	PSQ	K_Z (M^2/S)	K_H (M^2/S)	RH (%)	T (°C)
1	Pr-F-P	1.1	338.2	0 ± 0	0	G	0.34	9.72	83.6 ± 6.4	14.9 ± 2.4
	A-F-P	1.9 ± 0.8	35.7 ± 3.2	0 ± 0.0	22.3 ± 3.2	G	0.36	10.38	92.5 ± 1.0	10.7 ± 1.0
	F-P	1.0 ± 0.7	43.8 ± 9.8	23.5 ± 33.3	35.5 ± 21.9	G	0.4 ± 0.0	18.3 ± 12.2	94.6 ± 0.4	8.6 ± 0.3
	D-F-P	0.7	0	257.2	562.8	F	10.7	3150.00	95.3 ± 0.6	12.7 ± 1.8
	Po-F-P	1.8	19.4	604.4	974.2	D	120.8	9425.00	66.5 ± 7.6	21.9 ± 1.6
2	Pr-F-P	2.9	35.3	0	30	E	45.61	1304.00	78.8 ± 9.1	15.8 ± 1.0
	A-F-P	1.5 ± 0.5	72.7 ± 69.7	6.1 ± 10.5	36.6 ± 8.1	E	34.9 ± 8.7	998.9 ± 248.8	93.6 ± 1.5	12.5 ± 0.7
	F-P	1.8	319.4	47.1	110.8	F	12.81	365.40	97.0 ± 0.6	11.1 ± 0.4
	D-F-P	1.7	194.9	147.6	429.2	E	98.6	2756.70	91.8 ± 3.3	13.2 ± 0.8
	Po-F-P	2.2 ± 0.7	318.1 ± 21.5	426.6 ± 175.8	973.4 ± 984.7	D	181.4	5174.6	77.9 ± 6.7	16.5 ± 1.6
3	Pr-F-P	2.4	274.8	0	0	F	10.5	301.40	87.3 ± 1.0	10.4 ± 1.0
	A-F-P	2.8 ± 0.2	319.7 ± 10.9	0 ± 0	23.0 ± 2.8	F	19.0 ± 11.7	543.3 ± 333.2	93.2 ± 0.6	7.0 ± 0.2
	F-P	2.3	316.7	0	30	E	43.7	1250.00	92.9 ± 0.6	5.6 ± 0.8
	D-F-P	1.8	292.4	49.8	81.2	F	14.7	413.9	93.3 ± 0.8	5.3 ± 0.8
	Po-F-P	2.5 ± 0.4	276.3 ± 3.1	507.5 ± 205.3	930.3 ± 368.6	D	376.2 ± 174.5	8322.8 ± 4915.4	78.4 ± 7.4	13.4 ± 2.9
4	Pr-F-P	2	281.3	0	0	G	0.3	9.7	85.5 ± 4.4	10.6 ± 1.7
	A-F-P	1.3 ± 0.4	299.3 ± 10.7	0	26.0 ± 1.4	G	1.6 ± 1.8	47.2 ± 52.4	92.7 ± 0.8	7.0 ± 0.8
	F-P	1.4 ± 0.1	286.7 ± 6.2	12.5 ± 17.6	30.0 ± 14.1	G	2.6 ± 0.5	72.6 ± 15.9	94.4 ± 0.4	4.7 ± 0.6
	D-F-P	1.5	281.6	163.6	462.3	E	84.8 ± 110.6	2108.1 ± 2720.8	95.6 ± 0.3	7.3 ± 2.7
	Po-F-P	1.8	199	445.6	933.1	C	465.3	12840	73.8 ± 10.1	17.5 ± 1.6

Table 2
Fog processing period's average ± standard deviation meteorological parameters (wind speed (WS), wind direction (WD), solar radiation (SR), planetary boundary layer (PBL), F (fine fog droplets, diameter: 4–16 μm), M (Medium fog droplets, diameter: 16–22 μm), C (Coarse fog droplets, diameter: > 22 μm), LWC (fog droplets liquid water content), ALWC (aerosol liquid water content)).

Meteorology Parameter	Fog Processing Period				
	Pr-F-P	A-F-P	F-P	D-F-P	Po-F-P
RH (%)	83.7 ± 6.7	93.1 ± 1.2	94.4 ± 1.3	94.1 ± 2.1	75.5 ± 8.8
T (°C)	13.0 ± 2.9	10.1 ± 2.7	6.8 ± 2.4	8.8 ± 3.8	16.3 ± 3.8
WD (° from N)	232.4 ± 134.4	147.4 ± 140.2	216.2 ± 134.4	210.1 ± 124.0	218.1 ± 113.5
WS (m/s)	2.1 ± 0.8	1.9 ± 0.7	1.5 ± 0.6	1.5 ± 0.4	1.9 ± 0.5
PBL (m)	7.5 ± 15.0	25.2 ± 3.5	45.3 ± 34.2	399.6 ± 339.3	858.8 ± 426.5
SR (W/m^2)	0	0	19.9 ± 23.2	156.4 ± 109.1	479.4 ± 157.6
Fractional of Fog Droplets Number Concentration (%)		83.2 ± 6.0 (F)	69.7 ± 8.1 (F)	84.3 ± 15.8 (F)	
		6.3 ± 2.4 (M)	11.1 ± 3.0 (M)	5.1 ± 5.5 (M)	
		10.5 ± 4.1 (C)	19.2 ± 6.4 (C)	10.6 ± 11.9 (C)	
LWC (mg/m^3)		29.9 ± 15.9	173.7 ± 74.8	15.3 ± 20.5	
ALWC (μg/m^3)	207.9 ± 111.1	512.8 ± 128.9	440.0 ± 283.2	541.9 ± 220.4	144.1 ± 108.8

heterogeneous aqueous-phase production of nitrate through hydrolysis of N_2O_5 (Foltescu et al., 1996), and catalyzed by Fe and Mn metals (not measured here) (Rajput et al., 2016a). Cl is formed as a product of neutralization of HCl with NH_3 (Willison et al., 1989) and HCl get emitted mainly from coal combustion, biomass burning, and from the incineration of domestic and industrial wastes (Gupta and Mandariya, 2013). Their enhancement during Pr-F-P to A-F-P can be attributed to favorable meteorology and high BBOA mass. Subsequently, OA enhancement can attributed to an enhancement in different OA factors. Highest significant ($p < 0.05$) increment in OOA-1 by 36.1% followed by BBOA (51.3%), O-BBOA (31.7%), HOA (27.4%) was observed except OOA-2 in which slightly insignificant ($p > 0.05$) increment (1.6%) was recorded. The possible key role of these OA factors in variation is discussed in the subsequent text. When fog further get processed from A-F-P to F-P period, mass of all the species reduces drastically. OA was reduced by 39.3% while among all inorganic species, SO_4 got reduced with the highest rate (40.0%) followed by NO_3 (38.9%), Cl (35.9%), and NH_4 (35.0%), respectively. All these severe decrements in inorganic ions and OA mass was attributed to enhanced wet scavenging by the settling grown fog droplets (Gilardoni et al., 2014; Kaul et al., 2012) as evident from the enhanced number of medium and coarse fog droplets (Table 2). The fog scavenging efficiency of SO_4 (40.0%) was within the range of 18%–60%, as reported elsewhere (Facchini et al., 1999; Gilardoni et al., 2014; Hallberg et al., 1992). When fog further got processed to D-F-P, SO_4 was enhanced significantly ($p < 0.05$) with highest rate 60.8%, followed by Cl (50.4%), OA (32.4%), NH_4 (28.7%), and NO_3 (15.3%), respectively. This enhancement in Cl and OA mass can be explained by re-activation of local BB emission sources, supported by enhancement of BBOA by 134.5% as D-F-P belongs to early morning time. In the D-F-P, fog droplets started to evaporate which again enhance the number fraction of fine mode droplets and simultaneously suppresses the wet scavenging of interstitial aerosols. It appears that both within fine mode fog droplets as well interstitial aerosols (with high ALWC), aqueous-phase reactions of SO_2 and VOCs, were responsible for the enhanced aerosol mass as well as fractional increase of sulfate after droplet evaporation, and it is consistent with previous studies (Kaul et al., 2011; Kim et al., 2019). Also, the high ALWC, low T, and high RH indicate the aqueous-phase production pathway of NO_3 and SO_4 during D-F-P. However, from D-F-P to Po-F-P, a significant reduction in OA was observed possibly due to suppression of local BB emission, and vehicular

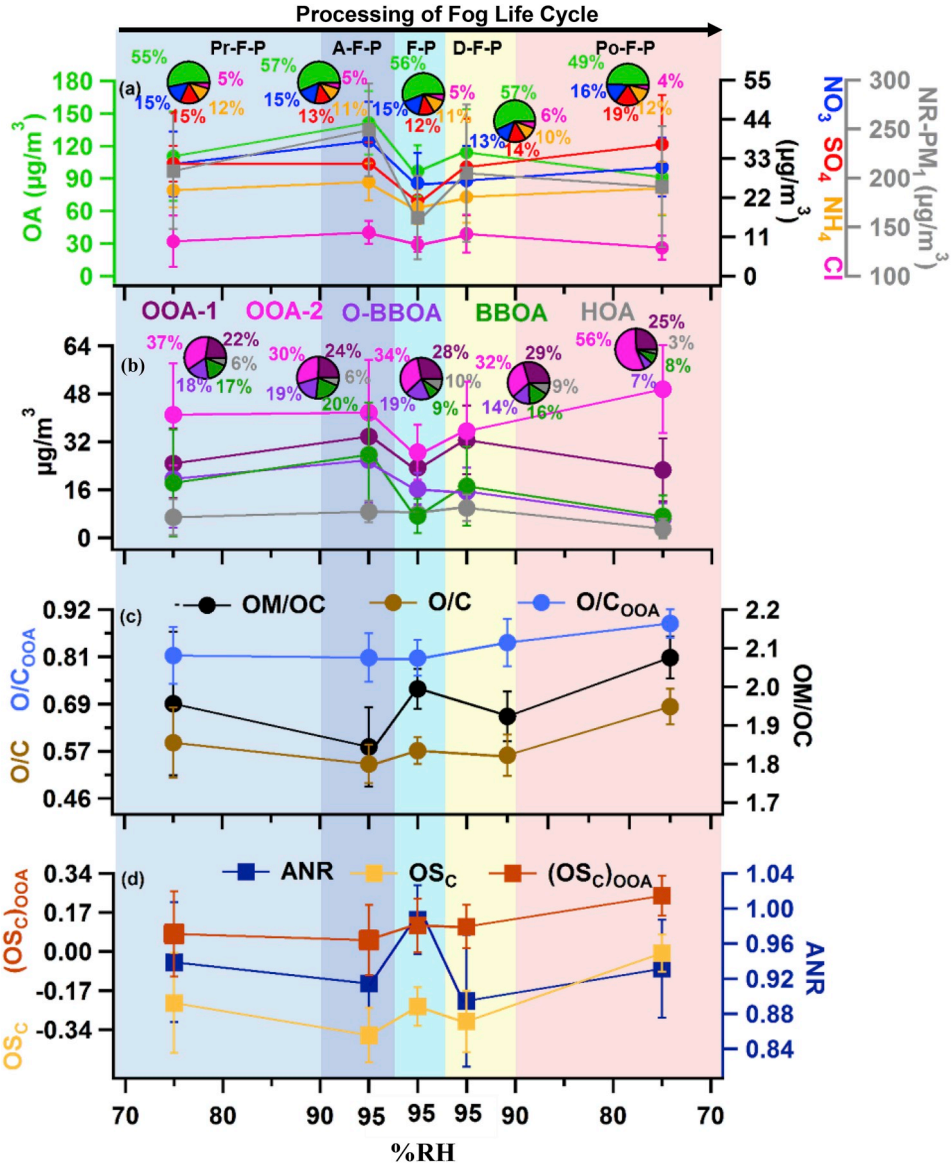

Fig. 1. The overview of the variation in overall (a) mass concentration of NR-PM_1 and its species with % contribution (pie charts), (b) mass concentration of various OA PMF factors with their % contribution into OA (pie charts), (c) bulk aerosol's O/C and OM/OC, and OOA's O/C_{OOA} ratio, and (d) aerosol neutralization ratio (ANR), bulk aerosol's OS_C, and OOA's $(OS_C)_{OOA}$ for the various fog processing periods during the course of fog life cycles. Different background color showing different fog processing periods. (For interpretation of the references to color in this figure legend, the reader is referred to the Web version of this article.)

emissions. These results can verified by significant ($p < 0.05$) reduction in BBOA and HOA by 58.3% and 69.8%, respectively. However, inorganic species (SO_4, NO_3, and NH_4) got increased significantly ($p < 0.05$) during the Po-F-P. The secondary inorganic species concentration peaked during Po-F-P, as photochemical activity resumed after fog dissipation (Chakraborty et al., 2015). Also, the significant enhancements in Po-F-P also suggest that aqueous-phase production of sulfate was faster than wet removal during the F-P period. In contrast, the decrease of nitrate and ammonium concentrations after F-P possibly resulted from wet deposition as well as evaporation at the higher temperature during the D-F-P and Po-F-P periods. D-F-P period is a crucial time for SO_4 production as compared to other fog processing periods.

3.3. *Effect of aqueous-phase processing on OA composition during various fog-processing periods*

Fig. 1 (b) shows the dynamic variation of mass concentration and fractional mass contribution of OA factors during different fog processing periods. Also, as reported in Table 2, ALWC also showed a significant ($p < 0.05$) variation during all fog processing periods followed by enhancement during A-F-P and D-F-P. However, decrement during F-P and Po-F-P indicates its potential impacts on aqueous-phase processing at different fog processing periods. The mass concentrations of OA factors was different among the five fog processing periods. The mass concentration of BBOA increased ($p < 0.05$) with sharply at a rate of 51.3% followed by OOA-1 (36.1%), O-BBOA (31.7%), HOA (27.4%), and OOA-2 (1.6%) as fog processed from Pr-F-P to A-F-P period (Fig. 1(b)). However, the overall fractional mass contribution of BBOA to OA got enhanced by 3% followed by OOA-1 (2%), and O-BBOA (1%), while OOA-2 decreased steeply by 7% during A-F-P. During this fog processing period, interstitial aerosol started to grow under favorable meteorology (low T and high RH) with high ALWC, and some fraction of them formed fine mode fog droplets which accounted for nearly 83.2% (as stated in Table 2). The interstitial aerosols were less competitive in taking up water molecules compared to the grown droplets. Majority of these grown droplets eventually settle down.

Hence, finer size interstitial aerosol present as the main surface area available for hygroscopic VOCs to condense upon. Therefore, more and more water-soluble VOCs and SVOCs from biomass emission start to dissolve or condense upon wet or semi-solid interstitial aerosol surface which results in the enhanced mass concentration of BBOA (McNeill, 2015). Subsequently, high BBOA mass is likely to trigger the aqueous-phase production pathway of OOA-1 (Fig. S6) and result in the significant ($p < 0.05$) enhancement in the aerosol mass concentration as well as its fractional contribution. An excellent correlation of OOA-1 with BBOA (as shown in Figs. S11(a) and (c)) likely indicates their similar local sources and/or support the possible pathway of BBOA transformation to OOA-1 through aqueous-phase processing. Also, O-BBOA was possibly contributing to OOA-1 supported by their good correlation (Figs. S11(b) and (d)). In contrast to aqueous-phase processing, a very well ($R^2 = 0.78$, $p < 0.05$) correlation of OOA-1 with ALWC (Fig. 2(a)) driven by anthropogenic secondary inorganic aerosol species (NO_3, SO_4, NH_4, and Cl), support its aqueous-phase processing (Gilardoni et al., 2016; Xu et al., 2017). Also, high loading of inorganic salts and OA in the presence of acidic medium (pH = 5.2 ± 4.4 (Pr-F-P) and pH = 1.4 ± 0.7 (A-F-P)) are typical of aerosols, creating favorable conditions for aqueous processing, selecting acid-catalyzed reactions (McNeill, 2015). Also, elevated OA mass concentration may lead to an OH-limited climate, could trigger the SOA (OOA-1) formation by glyoxal and methylglyoxal through dark reactions in aqueous aerosol (Ervens et al., 2011), supported by very nice correlation of OOA-1 with characteristic fragment ions of methylglyoxal ($C_2O_2^+$, $C_2H_2O_2^+$) as illustrated in Fig. 2(a). This statement can also be supported by a more significant fraction of f29 being observed within OOA-1 (Fig. S6) which represents a signal of CHO^+ characteristic ion. Also, the decrement in OOA-2 indicates its steady source and dominance of wet removal through the fine mode fog droplets. Further, when fog life cycle proceeds to F-P, all OA constituents decrease in a drastic manner which indicates their wet removal through settling of grown fog droplets (Gilardoni et al., 2014) as evident by increasing number of medium and coarse fog droplets (Table 2). The wet scavenging efficiency through grown fog droplets was highest for O-BBOA (37.2%) among all OOA factors followed by OOA-2 (31.6%) and OOA-1 (30.7%). However, it was highest for BBOA (73.5%) among all OA factors. This highest scavenging efficiency for BBOA and localized OOA-1 factor processed through aqueous-phase processing of BB emissions possibly indicate their water affinity nature (hygroscopic). Also, massive enhancement of OOA-2 in fractional mass contribution to OA from 30 to 34%, indicates the wet removal mechanism of other factors, i.e., OOA-1, O-BBOA, and BBOA, is much more dominant over their aqueous-phase production. The larger fog droplet size had a lower surface area for interaction with water-soluble VOCs, and SVOCs from

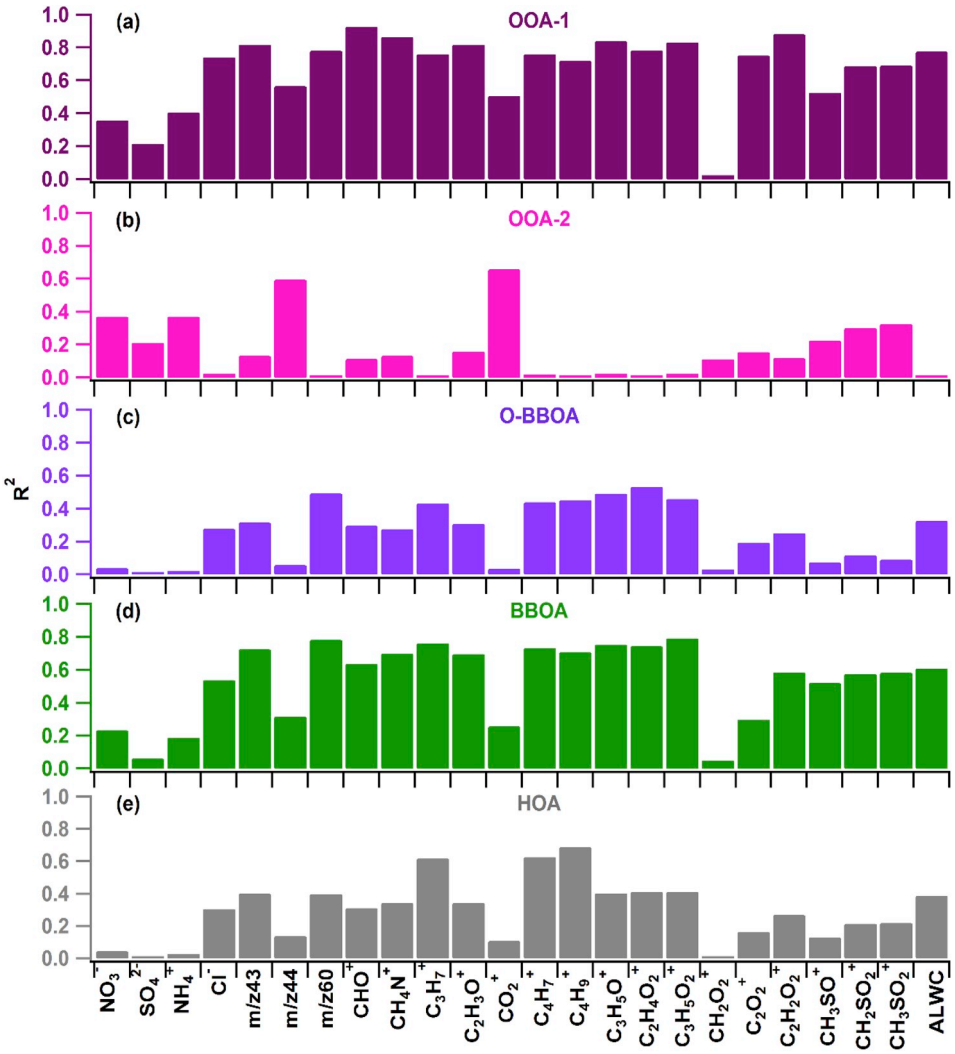

Fig. 2. Evidence of aqueous-phase processing. Correlation coefficients of (a) 1-OOA, (b) 2-OOA, (c) O-BBOA, (d) BBOA, and (e) HOA with inorganic species (NO_3^-, SO_4^{2-}, NH_4^+, and Cl^-), m/z (43, 44, and 60) and typical fragment ions (CH_4N^+, $C_3H_7^+$, $C_2H_3O^+$, CO_2^+, $C_4H_7^+$, $C_4H_9^+$, $C_3H_5O^+$, $C_2H_4O_2^+$, $C_3H_5O_2^+$, $CH_2O_2^+$, $C_2O_2^+$, $C_2H_2O_2^+$, CH_3SO^+, $CH_2SO_2^+$, $CH_3SO_2^+$, and aerosol liquid water content (ALWC).

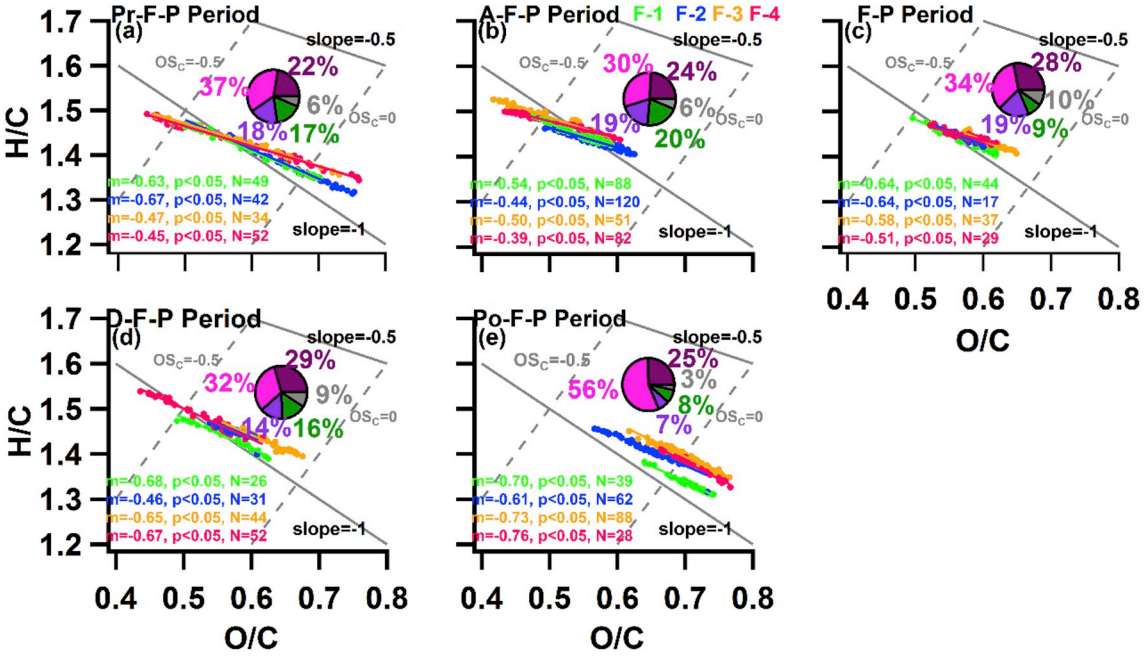

Fig. 3. Evolution of OA elemental ratio for (a) Pr-F-P, (b) A-F-P, (c) F-P, (d) D-F-P, and (e) Po-F-P fog processing periods during the fog life cycle. Each green, blue, orange and pink circle, text, and line (linear regression line) represent 1st (F-1), 15th (F-2), 22nd (F-3), and 23rd (F-4) January fog life cycles respectively. Pie chart represents average mass fractional contribution. (For interpretation of the references to color in this figure legend, the reader is referred to the Web version of this article.)

biomass emission as compared to comparatively fine droplets (during A-F-P). This larger droplet size suppressing the formation pathway over the wet scavenging through gravity settling could be the one reason for huge drop in mass as well as the fractional mass contribution of BBOA (Fig. 1(b), Table 2). In contrast to wet removal, more oxidized and more hygroscopic OOA is expected to be favorably scavenged as compared to primary OA factors (Gilardoni et al., 2014) which indicate that the excess and fast OOA production counterbalance the OOA scavenging. When fog ends and starts dissipating, all OA species get enhanced with significant ($p < 0.05$) rate followed by BBOA (134.5%), OOA-1 (39.5%), OOA-2 (24.6%), and HOA (23.8%) during D-F-P. However, O-BBOA observed insignificant ($p > 0.05$) drop in mass at the rate of 5%. The slowdown of wet removal rate can explain the enhancement rate of OOA factors during the D-F-P period. The higher rate of increment indicated the re-activation of local BB emissions and role of evaporated tiny fog droplet (Table 2), and aerosol with high ALWC (Table 2) which provide a larger surface area for partitioning of water-soluble VOCs and SVOCs into aerosol droplet surface. Further fog life cycle proceeds to Po-F-P, all OA species decrease except OOA-2, indicating its photochemical production during the daytime when temperature increases and ALWC decreases. Also, drop in mass as well as in fractional mass contribution to OA of O-BBOA and OOA-2 indicate the suppression of their aqueous-phase production pathway through BB emissions. These results indicate that aqueous-phase processing during the A-F-P and D-F-P periods appears to be a dominant pathway of the formation of OOA-1 and O-BBOA over wet removal. Successively during the F-P period, wet scavenging of OOA-1 and O-BBOA was dominating over their aqueous-phase production. To eliminate the effect of planetary boundary layer (PBL) on OA factors, we used HOA as a proxy (Xu et al., 2017). All OA factors showed variation throughout all the fog processing periods as illustrated in Fig. S9. PBL increases from Pr-F-P to Po-F-P (Table 2) so Pr-F-P was selected as a reference to further normalize the ratio. It indicates that changes in OA factors is not due to PBL dilution and vertical mixing.

Further, OOA-1 increasing trend during Pr-F-P to D-F-P indicates its production enhancement as illustrated in Fig. S9(b), further supporting our above findings. Also, O-BBOA showed increasing trend up-to F-P, while OOA-2 got enhanced during Po-F-P as shown in Fig. S8. O-BBOA upward trend (Fig. S9(b)) Pr-F-P to F-P indicates its nighttime aqueous-phase processing. The finding that OOA-1, OOA-2, O-BBOA, and BBOA get affected by aqueous-phase processing further is supported by their good to moderate or poor correlations with specific fragment ions and ALWC. Fig. 2 shows that OOA-2 is poorly correlated with characteristic fragment ions of methylglyoxal ($C_2O_2^+$, $C_2H_2O_2^+$), which are precursors of SOA in cloud processing pathways (Altieri et al., 2008; Carlton et al., 2007). Also, OOA-1 also showed excellent correlation with methanesulfonic acid (MSA) fragment ions (CH_3SO^+, $CH_2SO_2^+$, and $CH_3SO_2^+$) while BBOA showed good correlation. MSA is mostly an oxidation product of dimethyl sulfide (Barnes et al., 2006), or organo sulfate (OS) compounds (Farmer et al., 2010), can be enhanced by aqueous-phase processing (Ge et al., 2012). However, significant good correlation ($R^2 = 0.61$, $p < 0.05$) of BBOA and moderately good correlation ($R^2 = 0.33$, $p < 0.05$) of O-BBOA with ALWC also indicate their aqueous-phase production pathway. This good correlation of BBOA also indicates that aqueous-phase processing of primary biomass burning emissions plays a vital role in the formation of biomass burning aqueous-secondary organic aerosols. Above findings suggesting that OOA-1 is a good surrogate aqueous SOA (aqSOA) processed through BB emissions.

3.4. Effects of aqueous-phase processing on oxidative properties OA and evolution process during different fog processing periods

3.4.1. O/C ratio

Fig. 1(c) shows significant variations in bulk O/C ratio of OA throughout all fog processing periods as a response to the changes in OA composition. O/C ratio showed decrement by ~0.04 ($p < 0.05$) and ~0.01 ($p > 0.05$) during processing of fog cycle from Pr-F-P to A-F-P and F-P to D-F-P periods, respectively. While it increased by 0.04 ($p < 0.05$) and 0.12 ($p < 0.05$) during A-F-P to F-P and D-F-P to Po-F-P periods, respectively. Subsequently, this dynamic behavior of O/C is interestingly similar to that of f44 (as shown in Fig. 4(a) and b) (Cerully et al., 2015; Duplissy et al., 2011; Sorooshian et al., 2010) as well as with ANR (as shown in Fig. 2(d)) (Chakraborty et al., 2015). These

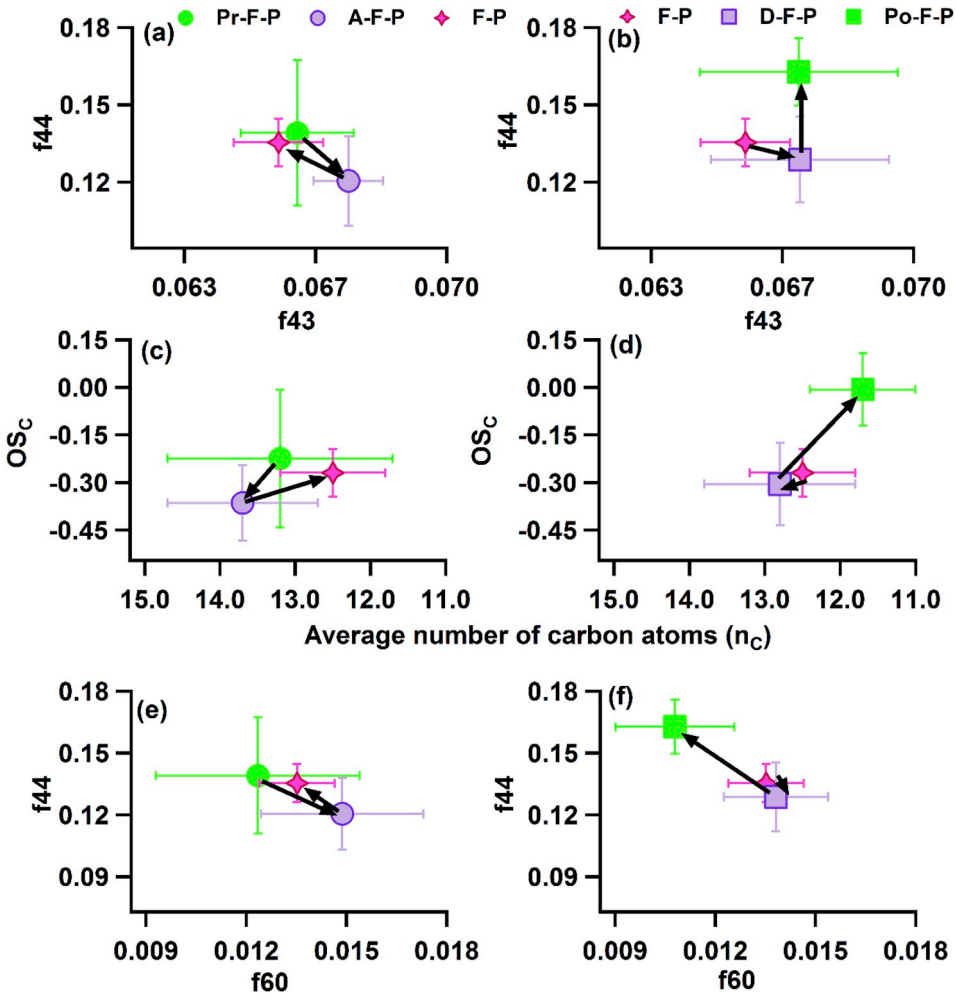

Fig. 4. OA evaluation (a) f44 vs. f43 plot for Pr-F-P to F-P, (b) f44 vs. f43 plot for F-P to Po-F-P, space plot of average carbon oxidation state (OS_C) and average number of carbon atoms (n_C) for (c) Pr-F-P to F-P and (d) F-P to Po-F-P, Plot of f44 (a marker of carboxylic acid) vs. f60 (a marker of biomass burning) for (e) Pr-F-P to F-P and (f) F-P to Po-F-P. Each marker and bar represent mean of the period and ± 1 standard deviation (σ) respectively. The black arrow represents the sequence of fog processing periods during processing of fog life cycle.

outcomes supported that aqueous-phase processing during the different fog processing periods in processing of fog life cycle alters the oxidation degree of OA by altering OA chemical composition (Chakraborty et al., 2015, 2016c; Lim et al., 2010). As illustrated in Fig. 1(c and e), it indicated that during the initial stage of fog formation (A-F-P) and fog dissipation stage (D-F-P) aerosol are most acidic (pH = 1.4 ± 0.7 (A-F-P) and pH = 2.0 ± 2.1 (D-F-P)) along with higher fraction of fine fog droplets (Table 2) which provides the platform to the dissolution of more and more organic VOCs/gases in liquid aerosol droplets. Subsequently, this acidic medium could be the significant factor in the enhancement of OOA-1 and O-BBOA, and BBOA, which results in overall decrement in O/C ratio of bulk aerosol. In addition to a healthier explanation of the effect of aqueous-phase processing on OOA during the processing of fog life cycle, we further calculated the O/C ratio of OOA for all fog processing periods. As shown in Fig. 1(c), O/C_{OOA} showed a remarkably different trend as bulk O/C. The variation in O/C_{OOA} was governed mainly by relative fractional mass contribution of OOA-1 and OOA-2 in OOA.

3.4.2. Van Krevelen slope and triangular plots

For better explaining the impacts of aqueous-phase processing on the OA transformation process and evaluation process, Van Krevelen (VK) slopes, triangular plots (f44 vs. f43), space plot of f44 vs. f60, average oxidation state of carbon (OS_C), and ammonium neutralization ratio (ANR) of OA were examined for different fog processing periods. The triangular plot (as shown in Fig. S5) and ternary diagram (as shown in Fig. S6) indicate the possible evolutionary pathway of aqueous-phase production of OOA-1. One possible evolution pathway can be BBOA to OOA-1 and second can be O-BBOA to OOA-1 during Pr-F-P to D-F-P. Also during Po-F-P, OOA-2 evolution pathway could be through OOA-1, O-BBOA, and other precursors. As shown in Figs. S4 and S6, oxygenated functional groups other than carboxylic groups, for example, ketone/aldehyde groups or alcohol groups (Chakraborty et al., 2015; Ng et al., 2010), as verified by the higher f29 value and mass fraction of CHO1 group also contributed to the high O/C values of OOA-1 (Lee et al., 2011).

Van Krevelen (VK) diagram is a cross space plot of hydrogen to carbon atomic ratio (H:C) and oxygen to carbon atomic ratio (O:C) of OA, provide insight to understand the reactions responsible for the addition of functional groups with the help of its slope (Heald et al., 2010; N L Ng et al., 2011). If during atmospheric processing of OA, an aliphatic carbon (−CH2−) replaced with a carbonyl group (−C(=O)−) suggests a loss of 2 hydrogen (H) atoms along with a gain of 1 oxygen (O) atom, and thus it is responsible for a slope of −2 (=-2/+1) in the VK diagram. Besides this, if the replacement of 1 H-atom with an alcohol group (−OH) results in an increment in oxygen without a change in hydrogen, and therefore results in a slope of 0 (=0/+1) in the VK plot. However, the simultaneous addition of both functional groups (−C(=O)− and −OH), forming a carboxylic acid (−COOH), and is responsible for a slope of −1 (=-1/+2) (Heald et al., 2010). In

contrast to the fragmentation process, a replacement of C—C bond cleavage with —COOH group, results in an intermediate slope of −0.5 (=-1/+2) in VK space (Daumit et al., 2013). However, comparatively shallow slope suggest either a greater tendency for —OH moieties addition or increase the importance of carbon-carbon bond breaking (fragmentation) reaction, which lead to relatively small changes in H:C. Further, OA observed significant variation in VK slope throughout all fog processing periods during all fog life cycles and follow consistently similar trend except F-3 event whereas during A-F-P to F-P period VK slope slightly increases ($p < 0.05$) in place of decreasing as shown in Fig. 3. However, overall variation in VK slope follows a similar trend as bulk O/C as shown in Fig. 1(c). Overall, among OA we observed shifting of VK slope to relatively shallow one as fog life cycle proceeded from Pr-F-P (−0.56 ± 0.11) to A-F-P (−0.47 ± 0.06) as illustrated in Fig. 3(a and b). This shift of VK slope shift toward relatively more shallow indicates the importance of functionalization —OH moieties and fragmentation reactions (N. L. Ng et al., 2011). Subsequently, comparatively shallow VK slope during A-F-P periods shows the increment of —OH group functionality which can be explained by an increase in mass and fractional mass contribution of OOA-1, O-BBOA, and BBOA factors. The shifting of OA position in the triangular plot (Fig. 4(a)) towards right downward (higher side of f43) support the above conclusion. Also, this shifting can verify with an increase in the negative value of OS_C (average oxidation state of carbon in OA) as well as a decrease of OS_C for OOA (Fig. 1(d)). Above results are also indicating the possibilities of formation of Humic-like substances (HULIS) and less oxidized semi-volatile oxygenated organic aerosol (SV-OOA) as OOA (Kroll et al., 2011). Also, high loading of biomass burning emission (Gilardoni et al., 2016) and acidic condition (Gao et al., 2004) during A-F-P, oligomerization can be a possible a path of OOA formation through aqueous-phase processing (De Haan et al., 2011). This conclusion can be further supported by Fig. 4 (c) which shows the overall shifting of OA towards left-downward ($p < 0.05$) (towards higher n_C and low OS_C), indicating oligomerization reaction and addition or functionalization of —OH group (Kroll et al., 2011). The reduction in f44 value as compared to higher f60 level (Fig. 4(e)) during A-F-P period also support this conclusion as f60 inversely affect the OA oxidation (Chakraborty et al., 2016c). Further, fog life cycle proceeds from A-F-P to F-P (Fig. 4(b and c)), VK slope reversely shift toward a steeper one from −0.47 ± 0.06 to −0.59 ± 0.06, indicating the dominance of either addition of more carbonyl (aldehyde/ketone) and —OH group at separate carbon atoms or –RCOOH moieties as compared to —OH moieties (Chakraborty et al., 2016c; Haddrell et al., 2015; N. L. Ng et al., 2011). Following conclusion verified by an enhancement in the fractional contribution of OOA-1 and OOA-2 to OA and reduction in BBOA. The significant ($p < 0.05$) shifting of f44 vs. f60 data point (Fig. 4 (e)) towards left-upward further support above results. However, OS_C observed significant ($p < 0.05$) increment while $(OS_C)_{OOA}$ remain nearly unchanged (Fig. 1(d)). In contrast to formation mechanism, the significant ($p < 0.05$) shifting of data point towards the right-upward side ($p < 0.05$) as shown in Fig. 4(c), indicate the dominance of fragmentation process with functionalization of –RCOOH or carbonyl (aldehyde/ketone) moieties during F-P periods. As a result, oxidation of bulk aerosol and OOA increase (Fig. 1(c)) and cause a decrease in acidity of aerosol (Fig. 1(d)). Further, during the D-F-P period, as shown in Fig. 3(d), overall VK slope got turned into relatively a steeper (−0.62 ± 0.11) one as compared to F-P (−0.59 ± 0.06), indicating possibility of the addition of more carbonyl (aldehyde/ketone) groups as compared to -RCOOH moieties. Following was further verified by the increment and decrement in f43 and f44, respectively (Fig. 4(b)). This result can also explain the enhancement of OOA-1 fractional contribution in OA by 1% over the 2% decrement of OOA-2 while all other OA factor mass concentration increased except O-BBOA. In context of formation mechanism during D-F-P (Fig. 4(d)), significant decrement in n_C ($p < 0.05$) and OS_C ($p < 0.05$) suggesting the possibility of oligomerization reactions along with carbonyl (aldehyde/ketone) moieties addition as enhancement in the acidic nature of aerosol (pH = 2.0 ± 2.1) can trigger the oligomerization reaction in aqueous-phase (Gao et al., 2004). The significant but slight decrement in O/C_{OOA} ratio could also explain it as oligomerization is a non-oxidation process (Daumit et al., 2013). Subsequently, continuous OA evolution during D-F-P to Po-F-P period and a shifting of VK slope toward comparatively steeper slope, indicates a continuous OA oxidation. Overall, significant ($p < 0.05$) increment of OOA-2 mass and fractional contribution in OA (Fig. 1(b)), which agrees well with significant ($p < 0.05$) enhancement in f44 whereas f43 remains constant (Fig. 4(b)). Note that shifting of OS_C ($p < 0.05$) towards left upper side with significant ($p < 0.05$) reduction in n_C as shown in Fig. 4(d) as well as an increment in $(OS_C)_{OOA}$ value (Fig. 1(d)), likely indicating formation of OOA via fragmentation process and functionalization of more –RCOOH moieties. In addition to significant reduction in primary BBOA, increase in f44 as compared to the significant reduction in f60 (Fig. 4(f)) further indicate the conversion of BB to OOA. Together with this our results suggest that aqueous-phase processing has different impacts on the formation of different OA components and their evolution process at different fog processing periods during fog life cycle.

4. Conclusions

Frequent and persistent fog episodes during winter time at IGP enhance OA loading as well as SOA via aqueous-phase processing. This study reports the effect aqueous-phase processing on OA during different fog processing periods of fog life cycles, regarding formation pathways, oxidative properties, and evolution pathways. Highest concentrations of $NR\text{-}PM_1$ were observed during A-F-P period (249.8 ± 47.8 μg/m^3) followed by Pr-F-P (207.8 ± 59.6 μg/m^3), D-F-P (205.0 ± 69.7 μg/m^3), Po-F-P (190.8 ± 61.6 μg/m^3) and F-P (153.1 ± 37.8 μg/m^3). Among all inorganic species, NO_3 was observed higher during Pr-F-P to F-P (before and during fog processing) while SO_4 during D-F-P to Po-F-P. Also, among all five fog processing periods, aerosol in A-F-P and D-F-P were observed acidic as well as with high ALWC. In addition, oxygen to carbon ratio (O/C) of OA and oxygenated organic aerosol (OOA) also varied during the all fog processing periods with a maximum during Po-F-P, however low O/C during A-F-P and D-F-P was observed to associate with high OA loading.

Our study indicating OOA-1 likely linked to biomass-burning emissions as its mass spectra reveal the slight presence of characteristic peaks of BBOA (m/z 60, m/z 73). It was supported by a good positive correlation of OOA-1 with BBOA and O-BBOA, and by the bivariate polar plot analysis which showed higher concentrations for relatively calm winds indicating local origins. In addition, the mass concentrations of the OOA-1 factor positively correlated with ALWC and typical fragments ions, i.e., $C_2H_2O_2^+$, $C_2O_2^+$, $CH_2O_2^+$ (fragment ions of methylglyoxal and glyoxal) and CH_3SO^+, $CH_2SO_2^+$, $CH_3SO_2^+$ (fragment ions of methanesulfonic acid (MSA)), suggesting its aqueous-phase formation from biomass burning emissions. It enhanced more during A-F-P and D-F-P under high biomass-burning emissions and acidic aerosol conditions. Our results are also suggesting; oligomerization mechanism could be significant for the formation of SOA along with functionalization of —OH and carbonyl (aldehyde/ketone) moieties during A-F-P and D-F-P, respectively accompanied by acidic aerosol as well as high aerosol liquid water content (ALWC) condition. However, the fragmentation process can be dominant along with functionalization of –RCOOH or carbonyl (aldehyde/ketone) and –RCOOH moieties during F-P and Po-F-P periods, respectively. Also, oxidation state (O/C ratio) of SOA enhanced during fog lifecycle processing from F-P to Po-F-P followed by the first decrement from Pr-F-P to F-P. Our results suggest that current SOA models should consider crucial A-F-P and D-F-P fog processing periods separately from pre-fog and post-fog, respectively to evaluate oxidative properties and mass concentration of SOA. These results may be beneficial in understanding the role of OA in wintertime fog formation chemistry and dissipation processes observed over the

central IGP and might fill the gap between measured and modeled SOA.

Declaration of interests

The authors declare that they have no known competing financial interests or personal relationships that could have appeared to influence the work reported in this paper.

Acknowledgment

We also acknowledge the support of IIT Kanpur for providing us with HR-ToF-AMS for PG research and teaching.

Appendix A. Supplementary data

Supplementary data to this article can be found online at https://doi.org/10.1016/j.atmosenv.2019.02.047.

References

Altieri, K.E., Seitzinger, S.P., Carlton, A.G., Turpin, B.J., Klein, G.C., Marshall, A.G., 2008. Oligomers formed through in-cloud methylglyoxal reactions: chemical composition, properties, and mechanisms investigated by ultra-high resolution FT-ICR mass spectrometry. Atmos. Environ. 42, 1476–1490. https://doi.org/10.1016/j.atmosenv.2007.11.015.

Arangio, A.M., Slade, J.H., Berkemeier, T., Pöschl, U., Knopf, D.A., Shiraiwa, M., 2015. Multiphase chemical kinetics of oh radical uptake by molecular organic markers of biomass burning aerosols: humidity and temperature dependence, surface reaction, and bulk diffusion. J. Phys. Chem. A 119, 4533–4544. https://doi.org/10.1021/jp510489z.

Barnes, I., Hjorth, J., Mihalopoulos, N., 2006. Dimethyl sulfide and dimethyl sulfoxide and their oxidation in the atmosphere. Chem. Rev. 106, 940–975. https://doi.org/10.1021/cr020529+.

Canagaratna, M.R., Jayne, J.T., Jimenez, J.L., Allan, J.D., Alfarra, M.R., Zhang, Q., Onasch, T.B., Drewnick, F., Coe, H., Middlebrook, A., Delia, A., Williams, L.R., Trimborn, A.M., Northway, M.J., DeCarlo, P.F., Kolb, C.E., Davidovits, P., Worsnop, D.R., 2007. Chemical and microphysical characterization of ambient aerosols with the aerodyne aerosol mass spectrometer. Mass Spectrom. Rev. 26, 185–222. https://doi.org/DOI 10.1002/mas.20115.

Carlton, A.G., Turpin, B.J., 2013. Particle partitioning potential of organic compounds is highest in the Eastern US and driven by anthropogenic water. Atmos. Chem. Phys. 13, 10203–10214. https://doi.org/10.5194/acp-13-10203-2013.

Carlton, A.G., Turpin, B.J., Altieri, K.E., Seitzinger, S., Reff, A., Lim, H.J., Ervens, B., 2007. Atmospheric oxalic acid and SOA production from glyoxal: results of aqueous photooxidation experiments. Atmos. Environ. 41, 7588–7602. https://doi.org/10.1016/j.atmosenv.2007.05.035.

Cerully, K.M., Bougiatioti, A., Hite, J.R., Guo, H., Xu, L., Ng, N.L., Weber, R., Nenes, A., 2015. On the link between hygroscopicity, volatility, and oxidation state of ambient and water-soluble aerosols in the southeastern United States. Atmos. Chem. Phys. 15, 8679–8694. https://doi.org/10.5194/acp-15-8679-2015.

Chakraborty, A., Bhattu, D., Gupta, T., Tripathi, S.N., Canagaratna, M.R., 2015. Real-time measurements of ambient aerosols in a polluted Indian city: sources, characteristics, and processing of organic aerosols during foggy and nonfoggy periods. J. Geophys. Res. Atmos. 120, 9006–9019. https://doi.org/10.1002/2015JD023419 (Received).

Chakraborty, A., Ervens, B., Gupta, T., Tripathi, S.N., 2016a. Characterization of organic residues of size- resolved fog droplets and their atmospheric Journal of Geophysical Research : Atmospheres. J. Geophys. Res. Atmos. 121, 4317–4332. https://doi.org/10.1002/2015JD024508 (Received).

Chakraborty, A., Ervens, B., Gupta, T., Tripathi, S.N., 2016b. Characterization of organic residues of size- resolved fog droplets and their atmospheric Journal of Geophysical Research : Atmospheres. J. Geophys. Res. Atmos. 4317–4332. https://doi.org/10.1002/2015JD024508 (Received).

Chakraborty, A., Gupta, T., 2010. Chemical characterization and source apportionment of submicron (PM1) aerosol in Kanpur Region, India. Aerosol Air Qual. Res. 10, 433–445. https://doi.org/10.4209/aaqr.2009.11.0071.

Chakraborty, A., Gupta, T., Tripathi, S.N., 2016c. Combined effects of organic aerosol loading and fog processing on organic aerosols oxidation, composition, and evolution. Sci. Total Environ. 573, 690–698. https://doi.org/10.1016/j.scitotenv.2016.08.156.

Chen, Q., Liu, Y., Donahue, N.M., Shilling, J.E., Martin, S.T., 2011. Particle-phase chemistry of secondary organic material: modeled compared to measured O:C and H:C Elemental ratios provide constraints. Environ. Sci. Technol. 45, 4763–4770. https://doi.org/10.1021/es104398s.

Choudhary, V., Rajput, P., Kumar, D., Kumar, A., 2018. Light absorption characteristics of brown carbon during foggy and non- foggy episodes over the Indo-Gangetic Plain. Atmos. Pollut. Res. 9, 494–501. https://doi.org/10.1016/j.apr.2017.11.012.

Daumit, K.E., Kessler, S.H., Kroll, J.H., 2013. Average chemical properties and potential formation pathways of highly oxidized organic aerosol. Faraday Discuss 165, 181. https://doi.org/10.1039/c3fd00045a.

De Haan, D.O., Hawkins, L.N., Kononenko, J.A., Turley, J.J., Corrigan, A.L., Tolbert, M.A., Jimenez, J.L., 2011. Formation of nitrogen-containing oligomers by methylglyoxal and amines in simulated evaporating cloud droplets. Environ. Sci. Technol. 45, 984–991. https://doi.org/10.1021/es102933x.

DeCarlo, P.F., Kimmel, J.R., Trimborn, A., Northway, M.J., Jayne, J.T., Aiken, A.C., Gonin, M., Fuhrer, K., Horvath, T., Docherty, K.S., Worsnop, D.R., Jimenez, J.L., 2006. Field-deployable, high-resolution, time-of-flight aerosol mass spectrometer. Anal. Chem. 78, 8281–8289. https://doi.org/10.1021/ac061249n.

Deng, H., Tan, H., Li, F., Cai, M., Chan, P.W., Xu, H., Huang, X., Wu, D., 2016. Impact of relative humidity on visibility degradation during a haze event: a case study. Sci. Total Environ. 569–570, 1149–1158. https://doi.org/10.1016/j.scitotenv.2016.06.190.

Deng, X., Tie, X., Wu, D., Zhou, X., Bi, X., Tan, H., Li, F., Jiang, C., 2008. Long-term trend of visibility and its characterizations in the Pearl River Delta (PRD) region, China. Atmos. Environ. Times 42, 1424–1435. https://doi.org/10.1016/j.atmosenv.2007.11.025.

Donahue, N.M., Robinson, A.L., Stanier, C.O., Pandis, S.N., 2006. Coupled partitioning, dilution, and chemical aging of semivolatile organics. Environ. Sci. Technol. 40, 2635–2643. https://doi.org/10.1021/es052297c.

Drewnick, F., Hings, S.S., DeCarlo, P., Jayne, J.T., Gonin, M., Fuhrer, K., Weimer, S., Jimenez, J.L., Demerjian, K.L., Borrmann, S., Worsnop, D.R., 2005. A new time-of-flight aerosol mass spectrometer (TOF-AMS) - instrument description and first field deployment. Aerosol Sci. Technol. 39, 637–658. https://doi.org/10.1080/02786820500182040.

Duplissy, J., De Carlo, P.F., Dommen, J., Alfarra, M.R., Metzger, A., Barmpadimos, I., Prevot, A.S.H., Weingartner, E., Tritscher, T., Gysel, M., Aiken, A.C., Jimenez, J.L., Canagaratna, M.R., Worsnop, D.R., Collins, D.R., Tomlinson, J., Baltensperger, U., 2011. Relating hygroscopicity and composition of organic aerosol particulate matter. Atmos. Chem. Phys. 11, 1155–1165. https://doi.org/10.5194/acp-11-1155-2011.

Eagleman, J.R., 1996. Air Pollution Meteorology. Trimedia 2nd edditi.

Ervens, B., Turpin, B.J., Weber, R.J., 2011. Secondary organic aerosol formation in cloud droplets and aqueous particles (aqSOA): a review of laboratory, field and model studies. Atmos. Chem. Phys. 11, 11069–11102. https://doi.org/10.5194/acp-11-11069-2011.

Facchini, M.C., Mircea, M., Fuzzi, S., Charlson, R.J., 1999. Cloud albedo enhancement by surface-active organic solutes in growing droplets. Nature 401, 257–259. https://doi.org/10.1038/45758.

Farmer, D.K., Matsunaga, A., Docherty, K.S., Surratt, J.D., Seinfeld, J.H., Ziemann, P.J., Jimenez, J.L., 2010. Response of an aerosol mass spectrometer to organonitrates and organosulfates and implications for atmospheric chemistry. Proc. Natl. Acad. Sci. 107, 6670–6675. https://doi.org/10.1073/pnas.0912340107.

Foltescu, V.L., Lindgren, E.S., Isakson, J., Oblad, M., Pacyna, J.M., Benson, S., 1996. Gas-to-particle conversion of sulphur and nitrogen compounds as studied at marine stations in northern Europe. Atmos. Environ. 30, 3129–3140.

France, O.B., France, C.G., Germany, C.H., Uk, A.J., 2013. Clouds and aerosols. In: Climate Change 2013 the Physical Science Basis: Working Group I Contribution to the Fifth Assessment Report of the Intergovernmental Panel on Climate Change, pp. 571–658. https://doi.org/10.1017/CBO9781107415324.016.

Frank, G., Martinsson, B.G., Cederfelt, S.I., Berg, O.H., Swietlicki, E., Wendisch, M., Yuskiewicz, B., Heintzenberg, J., Wiedensohler, A., Orsini, D., Stratmann, F., Laj, P., Ricci, L., 1998. Droplet formation and growth in polluted fogs. Contrib. Atmos. Phys. 71, 65–85.

Gao, S., Ng, N.G. a L., Keywood, M., Varutbangkul, V., Bahreini, R., Nenes, A., He, J., Yoo, K.Y., Beauchamp, J.L., Hodyss, R.P., Flagan, R.C., Seinfeld, J.H., 2004. Particle phase acidity and oligomer formation in secondary organic aerosol. Environ. Sci. Technol. 38, 6582–6589.

Ge, X., Zhang, Q., Sun, Y., Ruehl, C.R., Setyan, A., 2012. Effect of aqueous-phase processing on aerosol chemistry and size distributions in Fresno, California, during wintertime. Environ. Chem. 9, 221–235. https://doi.org/10.1071/EN11168.

Gelencsér, A., May, B., Simpson, D., Sánchez-Ochoa, A., Kasper-Giebl, A., Puxbaum, H., Caseiro, A., Pio, C.A., Legrand, M., 2007. Source apportionment of PM2.5 organic aerosol over Europe: primary/secondary, natural/anthropogenic, and fossil/biogenic origin. J. Geophys. Res. Atmos. 112, 1–12. https://doi.org/10.1029/2006JD008094.

Gilardoni, S., Massoli, P., Giulianelli, L., Rinaldi, M., Paglione, M., Pollini, F., Lanconelli, C., Poluzzi, V., Carbone, S., Hillamo, R., Russell, L.M., Facchini, M.C., Fuzzi, S., 2014. Fog scavenging of organic and inorganic aerosol in the po valley. Atmos. Chem. Phys. 14, 6967–6981. https://doi.org/10.5194/acp-14-6967-2014.

Gilardoni, S., Massoli, P., Paglione, M., Giulianelli, L., Carbone, C., Rinaldi, M., Decesari, S., Sandrini, S., Costabile, F., Gobbi, G.P., Pietrogrande, M.C., Visentin, M., Scotto, F., Fuzzi, S., Facchini, M.C., 2016. Direct observation of aqueous secondary organic aerosol from biomass-burning emissions. Proc. Natl. Acad. Sci. 113, 10013–10018. https://doi.org/10.1073/pnas.1602212113.

Gupta, T., Mandariya, A., 2013. Sources of submicron aerosol during fog-dominated wintertime at Kanpur. Environ. Sci. Pollut. Res. 20, 5615–5629. https://doi.org/10.1007/s11356-013-1580-6.

Haddrell, A.E., Davies, J.F., Reid, J.P., 2015. Dynamics of particle size on inhalation of environmental aerosol and impact on deposition fraction. Environ. Sci. Technol. 49, 14512–14521. https://doi.org/10.1021/acs.est.5b01930.

Hallberg, A., Ogren, J.A., Noone, K.J., Heintzenberg, J., Berner, A., Solly, I., Kruisz, C., Reischl, G., Fuzzi, S., Facchini, M.C., Hansson, H.-C., Wiedensohler, A., Svenningsson, I.B., 1992. Phase partitioning for different aerosol species in fog. Tellus B 44, 545–555. https://doi.org/10.1034/j.1600-0889.1992.t01-2-00008.x.

Hallquist, M., Wenger, J.C., Baltensperger, U., Rudich, Y., Simpson, D., Claeys, M., Dommen, J., Donahue, N.M., George, C., Goldstein, A.H., Hamilton, J.F., Herrmann, H., Hoffmann, T., Linuma, Y., Jang, M., Jenkin, M.E., Jimenez, J.L., Kiendler-Scharr, A., Maenhaut, W., McFiggans, G., Mentel, T.F., Monod, A., Pŕev̂ot, A.S.H., Seinfeld, J.H., Surratt, J.D., Szmigielski, R., Wildt, J., 2009. The formation, properties and

impact of secondary organic aerosol: current and emerging issues. Atmos. Chem. Phys. 9, 5155–5236.
Heald, C.L., Kroll, J.H., Jimenez, J.L., Docherty, K.S., Decarlo, P.F., Aiken, A.C., Chen, Q., Martin, S.T., Farmer, D.K., Artaxo, P., 2010. A simplified description of the evolution of organic aerosol composition in the atmosphere. Geophys. Res. Lett. 37, L08803. https://doi.org/10.1029/2010GL042737.
Herndon, S.C., Onasch, T.B., Wood, E.C., Kroll, J.H., Canagaratna, M.R., Jayne, J.T., Zavala, M.A., Knighton, W.B., Mazzoleni, C., Dubey, M.K., Ulbrich, I.M., Jimenez, J.L., Seila, R., de Gouw, J.A., de Foy, B., Fast, J., Molina, L.T., Kolb, C.E., Worsnop, D.R., 2008. Correlation of secondary organic aerosol with odd oxygen in Mexico City. Geophys. Res. Lett. 35, 1–6. https://doi.org/10.1029/2008GL034058.
Hodas, N., Zuend, A., Mui, W., Flagan, R.C., Seinfeld, J.H., 2015. Influence of particle-phase state on the hygroscopic behavior of mixed organic-inorganic aerosols. Atmos. Chem. Phys. 15, 5027–5045. https://doi.org/10.5194/acp-15-5027-2015.
Jayne, J.T., Leard, D.C., Zhang, X., Davidovits, P., Smith, K.A., Kolb, C.E., Worsnop, D.R., 2000. Development of an aerosol mass spectrometer for size and composition analysis of submicron particles. Aerosol Sci. Technol. 33, 49–70. https://doi.org/10.1080/027868200410840.
Jimenez, J.L., Canagaratna, M.R., Donahue, N.M., Pŕ eŷ ot, A.S.H., Zhang, Q., Kroll, J.H., DeCarlo, P.F., Allan, J.D., Coe, H., Ng, N.L., Aiken, A.C., Docherty, K.D., Ulbrich, I.M., Grieshop, A.P., Robinson, A.L., Duplissy, J., Smith, J.D., Wilson, K.R., Lanz, V.A., Hueglin, C., Sun, Y.L., Laaksonen, A., Raatikainen, T., Rautiainen, J., Vaattovaara, P., Ehn, M., Kulmala, M., Tomlinson, J.M., Collins, D.R., Cubison, M.J., Dunlea, E.J., Huffman, J.A., Onasch, T.B., Alfarra, M.R., Williams, P.I., Bower, K., Kondo, Y., Schneider, J., Drewnick, F., Borrmann, S., Weimer, S., Demerjian, K., Salcedo, D., Cottrell, L., Griffin, R., Takami, A., Miyoshi, T., Hatakeyama, S., Shimono, A., Sun, J.Y., Zhang, Y.M., Dzepina, K., Kimmel, J.R., Sueper, D., Jayne, J.T., Herndon, S.C., Trimborn, A.M., Williams, L.R., Wood, E.C., Kolb, C.E., Baltensperger, U., Worsnop, D.R., 2009a. Evolution of organic aerosols in the atmosphere. Science 326 (80), 1525–1529. https://doi.org/10.1126/science.1180353.
Jimenez, J.L., Canagaratna, M.R., Donahue, N.M., Prevot, a. S.H., Zhang, Q., Kroll, J.H., DeCarlo, P.F., Allan, J.D., Coe, H., Ng, N.L., Aiken, a. C., Docherty, K.S., Ulbrich, I.M., Grieshop, A.P., Robinson, a. L., Duplissy, J., Smith, J.D., Wilson, K.R., Lanz, V. a., Hueglin, C., Sun, Y.L., Tian, J., Laaksonen, A., Raatikainen, T., Rautiainen, J., Vaattovaara, P., Ehn, M., Kulmala, M., Tomlinson, J.M., Collins, D.R., Cubison, M.J., Dunlea, E.J., Huffman, J.A., Onasch, T.B., Alfarra, M.R., Williams, P.I., Bower, K., Kondo, Y., Schneider, J., Drewnick, F., Borrmann, S., Weimer, S., Demerjian, K., Salcedo, D., Cottrell, L., Griffin, R., Takami, A., Miyoshi, T., Hatakeyama, S., Shimono, A., Sun, J.Y., Zhang, Y.M., Dzepina, K., Kimmel, J.R., Sueper, D., Jayne, J.T., Herndon, S.C., Trimborn, a. M., Williams, L.R., Wood, E.C., Middlebrook, A.M., Kolb, C.E., Baltensperger, U., Worsnop, D.R., Dunlea, J., Huffman, J.A., Onasch, T.B., Alfarra, M.R., Williams, P.I., Bower, K., Kondo, Y., Schneider, J., Drewnick, F., Borrmann, S., Weimer, S., Demerjian, K., Salcedo, D., Cottrell, L., Griffin, R., Takami, A., Miyoshi, T., Hatakeyama, S., Shimono, A., Sun, J.Y., Zhang, Y.M., Dzepina, K., Kimmel, J.R., Sueper, D., Jayne, J.T., Herndon, S.C., Trimborn, a. M., Williams, L.R., Wood, E.C., Middlebrook, A.M., Kolb, C.E., Baltensperger, U., Worsnop, D.R., Dunlea, E.J., Huffman, J.A., Onasch, T.B., Alfarra, M.R., Williams, P.I., Bower, K., Kondo, Y., Schneider, J., Drewnick, F., Borrmann, S., Weimer, S., Demerjian, K., Salcedo, D., Cottrell, L., Griffin, R., Takami, A., Miyoshi, T., Hatakeyama, S., Shimono, A., Sun, J.Y., Zhang, Y.M., Dzepina, K., Kimmel, J.R., Sueper, D., Jayne, J.T., Herndon, S.C., Trimborn, a. M., Williams, L.R., Wood, E.C., Middlebrook, A.M., Kolb, C.E., Baltensperger, U., Worsnop, D.R., Dunlea, J., Huffman, J.A., Onasch, T.B., Alfarra, M.R., Williams, P.I., Bower, K., Kondo, Y., Schneider, J., Drewnick, F., Borrmann, S., Weimer, S., Demerjian, K., Salcedo, D., Cottrell, L., Griffin, R., Takami, A., Miyoshi, T., Hatakeyama, S., Shimono, A., Sun, J.Y., Zhang, Y.M., Dzepina, K., Kimmel, J.R., Sueper, D., Jayne, J.T., Herndon, S.C., Trimborn, a. M., Williams, L.R., Wood, E.C., Middlebrook, A.M., Kolb, C.E., Baltensperger, U., Worsnop, D.R., 2009b. Evolution of organic aerosols in the atmosphere. Science 80 (326), 1525–1529. https://doi.org/10.1126/science.1180353.
Jimenez, J.L., Jayne, J.T., Shi, Q., Kolb, C.E., Worsnop, D.R., Yourshaw, I., Seinfeld, J.H., Flagan, R.C., Zhang, X., Smith, K.A., Morris, J.W., Davidovits, P., 2003. Ambient aerosol sampling using the aerodyne aerosol mass spectrometer. J. Geophys. Res. 108, 8425. https://doi.org/10.1029/2001JD001213.
Kaul, D.S., Gupta, T., Tripathi, S.N., 2012. Chemical and microphysical properties of the aerosol during foggy and nonfoggy episodes: a relationship between organic and inorganic content of the aerosol. Atmos. Chem. Phys. Discuss. 12, 14483–14524. https://doi.org/10.5194/acpd-12-14483-2012.
Kaul, D.S., Gupta, T., Tripathi, S.N., Tare, V., Collett, J.L., 2011. Secondary organic aerosol: a comparison between foggy and nonfoggy days. Environ. Sci. Technol. 45, 7307–7313. https://doi.org/10.1021/es201081d.
Kim, H., Collier, S., Ge, X., Xu, J., Sun, Y., Jiang, W., Wang, Y., Herckes, P., Zhang, Q., 2019. Chemical processing of water-soluble species and formation of secondary organic aerosol in fogs. Atmos. Environ. 200, 158–166. https://doi.org/10.1016/j.atmosenv.2018.11.062.
Koop, T., Bookhold, J., Shiraiwa, M., Pöschl, U., 2011. Glass transition and phase state of organic compounds: dependency on molecular properties and implications for secondary organic aerosols in the atmosphere. Phys. Chem. Chem. Phys. 13, 19238–19255. https://doi.org/10.1039/c1cp22617g.
Kroll, J.H., Donahue, N.M., Jimenez, J.L., Kessler, S.H., Canagaratna, M.R., Wilson, K.R., Altieri, K.E., Mazzoleni, L.R., Wozniak, A.S., Bluhm, H., Mysak, E.R., Smith, J.D., Kolb, C.E., Worsnop, D.R., 2011. Carbon oxidation state as a metric for describing the chemistry of atmospheric organic aerosol. Nat. Chem. 3, 133–139. https://doi.org/10.1038/nchem.948.
Lee, A.K.Y., Herckes, P., Leaitch, W.R., MacDonald, A.M., Abbatt, J.P.D., 2011. Aqueous OH oxidation of ambient organic aerosol and cloud water organics: formation of highly oxidized products. Geophys. Res. Lett. 38, 2–6. https://doi.org/10.1029/2011GL047439.
Li, Y.J., Lee, B.Y.L., Yu, J.Z., Ng, N.L., Chan, C.K., 2013. Evaluating the degree of oxygenation of organic aerosol during foggy and hazy days in Hong Kong using high-resolution time-of-flight aerosol mass spectrometry (HR-ToF-AMS). Atmos. Chem. Phys. 13, 8739–8753. https://doi.org/10.5194/acp-13-8739-2013.
Lim, Y.B., Tan, Y., Perri, M.J., Seitzinger, S.P., Turpin, B.J., 2010. Aqueous chemistry and its role in secondary organic aerosol (SOA) formation. Atmos. Chem. Phys. 10, 10521–10539. https://doi.org/10.5194/acp-10-10521-2010.
McNeill, V.F., 2015. Aqueous organic chemistry in the atmosphere: sources and chemical processing of organic aerosols. Environ. Sci. Technol. 49, 1237–1244. https://doi.org/10.1021/es5043707.
Meng, J.W., Yeung, M.C., Li, Y.J., Lee, B.Y.L., Chan, C.K., 2014. Size-resolved cloud condensation nuclei (CCN) activity and closure analysis at the HKUST Supersite in Hong Kong. Atmos. Chem. Phys. 14, 10267–10282. https://doi.org/10.5194/acp-14-10267-2014.
Ng, N.L., Canagaratna, M.R., Jimenez, J.L., Chhabra, P.S., Seinfeld, J.H., Worsnop, D.R., 2011. Changes in organic aerosol composition with aging inferred from aerosol mass spectra. Atmos. Chem. Phys. 11, 6465–6474. https://doi.org/10.5194/acp-11-6465-2011.
Ng, N.L., Canagaratna, M.R., Zhang, Q., Jimenez, J.L., Tian, J., Ulbrich, I.M., Kroll, J.H., Docherty, K.S., Chhabra, P.S., Bahreini, R., Murphy, S.M., Seinfeld, J.H., Hildebrandt, L., Donahue, N.M., Decarlo, P.F., Lanz, V.A., Prévôt, A.S.H., Dinar, E., Rudich, Y., Worsnop, D.R., 2010. Organic aerosol components observed in northern hemispheric datasets from aerosol mass spectrometry. Atmos. Chem. Phys. 10, 4625–4641. https://doi.org/10.5194/acp-10-4625-2010.
Nguyen, T.K.V., Capps, S.L., Carlton, A.G., 2015. Decreasing aerosol water is consistent with OC trends in the Southeast U.S. Environ. Sci. Technol. 49, 7843–7850. https://doi.org/10.1021/acs.est.5b00828.
Parikh, H.M., Carlton, A.G., Vizuete, W., Kamens, R.M., 2011. Modeling secondary organic aerosol using a dynamic partitioning approach incorporating particle aqueous-phase chemistry. Atmos. Environ. 45, 1126–1137. https://doi.org/10.1016/j.atmosenv.2010.11.027.
Rai, P., Chakraborty, A., Mandariya, A.K., Gupta, T., 2016. Composition and source apportionment of PM1at urban site Kanpur in India using PMF coupled with CBPF. Atmos. Res. 178–179, 506–520. https://doi.org/10.1016/j.atmosres.2016.04.015.
Rajput, P., Gupta, T., Kumar, A., 2016a. The diurnal variability of sulfate and nitrate aerosols during wintertime in the Indo-Gangetic Plain: implications for heterogeneous phase chemistry. RSC Adv. 6, 89879–89887. https://doi.org/10.1039/C6RA19595D.
Rajput, P., Mandaria, A., Kachawa, L., Singh, D.K., Singh, A.K., Gupta, T., 2016b. Chemical characterisation and source apportionment of PM1during massive loading at an urban location in Indo-Gangetic Plain: impact of local sources and long-range transport. Tellus Ser. B Chem. Phys. Meteorol. 68. https://doi.org/10.3402/tellusb.v68.30659.
Rajput, P., Singh, D.K., Singh, A.K., Gupta, T., 2018. Chemical composition and source-apportionment of sub-micron particles during wintertime over Northern India: new insights on influence of fog-processing. Environ. Pollut. 233, 81–91. https://doi.org/10.1016/j.envpol.2017.10.036.
Robinson, A.L., Donahue, N.M., Rogge, W.F., 2006. Photochemical oxidation and changes in molecular composition of organic aerosol in the regional context. J. Geophys. Res. Atmos. 111, 1–15. https://doi.org/10.1029/2005JD006265.
Robinson, A.L., Donahue, N.M., Shrivastava, M.K., Weitkamp, E.A., Sage, A.M., Grieshop, A.P., Lane, T.E., Pierce, J.R., Pandis, S.N., 2007. Rethinking organic aerosols: semivolatile emissions and photochemical aging. Science 315 (80), 1259–1262. https://doi.org/10.1126/science.1133061.
Satish, R., Shamjad, P., Thamban, N., Tripathi, S., Rastogi, N., 2017. Temporal characteristics of brown carbon over the central indo-gangetic plain. Environ. Sci. Technol. 51, 6765–6772. https://doi.org/10.1021/acs.est.7b00734.
Seinfeld, J.H., Pandis, S.N., 2006. Atmospheric Cemistry and Physics: from Air Pollution to Climate Change, second ed. John Wiley & Sons, Inc.
Shamjad, P.M., Tripathi, S.N., Thamban, N.M., Vreeland, H., 2016. Refractive index and absorption attribution of highly absorbing brown carbon aerosols from an urban Indian city-Kanpur. Sci. Rep. 6, 1–7. https://doi.org/10.1038/srep37735.
Shen, X.J., Sun, J.Y., Zhang, X.Y., Zhang, Y.M., Zhang, L., Che, H.C., Ma, Q.L., Yu, X.M., Yue, Y., Zhang, Y.W., 2015. Characterization of submicron aerosols and effect on visibility during a severe haze-fog episode in Yangtze River Delta, China. Atmos. Environ. 120, 307–316. https://doi.org/10.1016/j.atmosenv.2015.09.011.
Singh, D.K., Gupta, T., 2016. Role of transition metals with water soluble organic carbon in the formation of secondary organic aerosol and metallo-organics in PM1sampled during post monsoon and pre-winter time. J. Aerosol Sci. 94, 56–69. https://doi.org/10.1016/j.jaerosci.2016.01.002.
Singh, V.P., Gupta, T., Tripathi, S.N., Jariwala, C., Das, U., 2011. Experimental study of the effects of environmental and fog condensation nuclei parameters on the rate of fog formation and dissipation using a new laboratory scale fog generation facility. Aerosol Air Qual. Res. 11, 140–154. https://doi.org/10.4209/aaqr.2010.08.0071.
Sorooshian, A., Murphy, S.M., Hersey, S., Bahreini, R., Jonsson, H., Flagan, R.C., Seinfeld, J.H., 2010. Constraining the contribution of organic acids and AMS m/z 44 to the organic aerosol budget: on the importance of meteorology, aerosol hygroscopicity, and region. Geophys. Res. Lett. 37, 1–5. https://doi.org/10.1029/2010GL044951.
Sun, Y., Du, W., Fu, P., Wang, Q., Li, J., Ge, X., Zhang, Q., Zhu, C., Ren, L., Xu, W., Zhao,

J., Han, T., Worsnop, D.R., Wang, Z., 2016. Primary and secondary aerosols in Beijing in winter: sources, variations and processes. Atmos. Chem. Phys. 16, 8309–8329. https://doi.org/10.5194/acp-16-8309-2016.

Sun, Y., Wang, Z., Fu, P., Jiang, Q., Yang, T., Li, J., Ge, X., 2013. The impact of relative humidity on aerosol composition and evolution processes during wintertime in Beijing, China. Atmos. Environ. Times 77, 927–934. https://doi.org/10.1016/j.atmosenv.2013.06.019.

Willison, M.J., Clarke, A.G., Zeki, E.M., 1989. Chloride aerosols in central northern England. Atmos. Environ. 23, 2231–2239. https://doi.org/10.1016/0004-6981(89)90185-6.

Wu, Y., Ge, X., Wang, J., Shen, Y., Ye, Z., Ge, S., Wu, Y., Yu, H., Chen, M., 2018. Formation and characteristics of secondary aerosols in an industrialized environment during cold seasons. Atmos. Chem. Phys. Discuss. https://doi.org/10.5194/acp-2018-75.

Xu, J., Shi, J., Zhang, Q., Ge, X., Canonaco, F., Prévôt, A.S.H., Vonwiller, M., Szidat, S., Ge, J., Ma, J., An, Y., Kang, S., Qin, D., 2016. Wintertime organic and inorganic aerosols in Lanzhou, China: sources, processes, and comparison with the results during summer. Atmos. Chem. Phys. 16, 14937–14957. https://doi.org/10.5194/acp-16-14937-2016.

Xu, W., Han, T., Du, W., Wang, Q., Chen, C., Zhao, J., Zhang, Y., Li, J., Fu, P., Wang, Z., Worsnop, D.R., Sun, Y., 2017. Effects of aqueous-phase and photochemical processing on secondary organic aerosol formation and evolution in Beijing, China. Environ. Sci. Technol. 51, 762–770. https://doi.org/10.1021/acs.est.6b04498.

Zhang, Q., Jimenez, J.L., Worsnop, D.R., Canagaratna, M., 2007. Article A Case Study of Urban Particle Acidity and its Influence on Secondary Organic Aerosol A Case Study of Urban Particle Acidity and its Influence on Secondary Organic Aerosol 3213–3219. https://doi.org/10.1021/es061812j.

Zhou, Y., Zhang, H., Parikh, H.M., Chen, E.H., Rattanavaraha, W., Rosen, E.P., Wang, W., Kamens, R.M., 2011. Secondary organic aerosol formation from xylenes and mixtures of toluene and xylenes in an atmospheric urban hydrocarbon mixture : water and particle seed effects (II). Atmos. Environ. 45, 3882–3890. https://doi.org/10.1016/j.atmosenv.2010.12.048.